Theor Chem Acc (2007) 117:1105–1120
DOI 10.1007/s00214-006-0223-0

REGULAR ARTICLE

Problems in molecular dynamics of condensed phases

Vincenzo Schettino · Riccardo Chelli · Simone Marsili · Alessandro Barducci · Cristian Faralli · Marco Pagliai · Piero Procacci · Gianni Cardini

Received: 29 September 2006 / Accepted: 13 October 2006 / Published online: 4 January 2007

Abstract A review of the recent theoretical and computational activity at the Chemistry Department of the University of Firenze in the field of molecular simulations of condensed phases is reported. The topics considered include quantitative methods for accurate free energy calculations, molecular dynamics of liquids and ionic solutions, chemical reactions in solutions, phase transformations and polymerization reactions at high pressures.

Keywords Simulations · Free energy · Prions · Chemical reactions · Hydrogen bonding · High-pressure reactivity

1 Introduction

Molecular dynamics (MD) simulation methods [1] are established since a long time as a powerful tool to analyze structural and dynamic properties of complex systems and condensed phases. Roughly speaking, MD simulations serve the twofold purpose of providing macroscopic properties, that can be of importance in direct connection with experimental findings, and of enlightening microscopic and atomistic details of the dynamic behavior that, in many cases, are hard to be directly sorted out from experimental data. Although the application of MD to condensed phases already has a long history and many relevant results have actually been obtained, research is currently carried out in many laboratories to implement the method, also taking advantage of the continuously increasing computational facilities, beyond the simple modeling approach toward a more realistic representation of the chemical and physical systems. The first facet of these efforts is concerned with the setting up of more appropriate interatomic interaction potentials, particularly in the case of systems or phenomena where a substantial rearrangement of the electron distribution takes place (like phase transformations, chemical reactions, very strong intermolecular interactions). In this respect, the development of first principles MD approaches [2] has been a fundamental break-through, even though at the expense of a major computational burden. A second important area of development is variously connected with the feasible length of the simulation runs that can preclude an efficient exploration of the phase space regions of interest. This is certainly the case for complex systems, like biological systems, and for condensed phases (like solids), where high energy barriers have to be overcome and the phenomena of interest can be classified as rare events occurring on a time scale much longer than the simulation time. To this purpose, several accelerating and non conventional sampling procedures have been proposed to allow for the overcoming of the potential barriers, a complete reconstruction of the energy surfaces and quantitative evaluations of free energies.

The recent computational activity of the Molecular Spectroscopy Laboratory in the Department of Chemistry of the University of Firenze has been concerned with several aspects of the MD simulation outlined earlier.

V. Schettino (✉) · R. Chelli · S. Marsili · A. Barducci · C. Faralli · M. Pagliai · P. Procacci · G. Cardini
Laboratorio di Spettroscopia Molecolare, Dipartimento di Chimica, Università di Firenze, Via della Lastruccia 3, Sesto Fiorentino, Italy
e-mail: vincenzo.schettino@unifi.it

V. Schettino · R. Chelli · S. Marsili · A. Barducci · C. Faralli · M. Pagliai · P. Procacci · G. Cardini
European Laboratory for Non-linear Spectroscopy (LENS), Via Nello Carrara 1, Sesto Fiorentino, Italy

In several cases, and in particular, with reference to the ultrafast dynamics of liquids and solutions, to phase transformations in solids and to chemical reactions at very high pressures, the computational activity has been paralleled by the experimental work carried at the European Laboratory for non-linear Spectroscopy (LENS) of the University of Firenze. In the following, we describe the main results that have been obtained in the areas of free energy calculations (Sect. 2), of the dynamics of biomolecules (Sect. 3), of the structure and dynamics of liquids (Sect. 4) and ionic solutions (Sect. 5), of phase transformations at high pressures (Sect. 7), and of chemical reactions in solution at ambient pressure (Sect. 6) and at very high pressures (Sect. 8).

2 Quantitative methods for free energy calculations

Quantitative determination of free energy surfaces (FESs) of complex systems has become a feasible task mainly in the last decade. In this respect, Boltzmann sampling is a brute force method that actually allows free energy determination only in a limited phase space region or for systems made of a small number of atoms. In our laboratory we recently used Boltzmann sampling to recover the FES of pairs of aromatic (amino acid-type) residues immersed in solvents of different polarity [3,4]. The purpose was to mimic the mutual interaction of aromatic residues in hydrophilic and hydrophobic environments typical of the surface and core of proteins, respectively.

To improve the sampling capabilities of computer simulations, a number of non-Boltzmann sampling methods have been devised in the recent years. We actually used a non-Boltzmann sampling method to calculate the free energy curve along a β-sheet reaction coordinate of the mouse prion protein (see discussion in Sect. 3). The efficiency of non-Boltzmann sampling methods can be greatly improved, as in a number of proposed algorithms [5–9], by an external force or potential that explicitly evolves in time "learning" from the foregoing part of a trajectory in phase space, finally reaching a stationary solution when a uniform sampling is obtained. Unfortunately, these kinds of approach to free energy reconstruction generally suffer from the need to set a number of system-dependent parameters by means of a trial and error procedure [9–13].

2.1 From non equilibrium to equilibrium dynamics through Self-Healing Umbrella Sampling

In order to introduce a general, system-independent algorithm for studying free energy differences, we recently proposed the Self-Healing Umbrella Sampling method [14] (SHUS). For a system in the canonical ensemble, the free energy $A(s)$ along a generic n-dimensional reaction coordinate $s(\mathbf{r})$ (where $\mathbf{r}$ is the vector of the coordinates of the system) is given by

$$A(s) = -k_B T \ln \rho(s), \tag{1}$$

where $\rho(s)$ is the probability density function along s. The slow sampling of the reaction coordinate, compared with the accessible simulation time scale, often precludes a straightforward evaluation of the function $\rho(s)$ through Boltzmann sampling and standard MD techniques. In the SHUS method, an external, explicitly time dependent potential $V(s,t)$ is added to the real Hamiltonian $H(\mathbf{r})$, in order to reach a uniform sampling of the reaction coordinate. The function

$$\rho(s,t) = \frac{\int_0^t \delta[s - s(\tau)]\, \rho(s,\tau) \mathrm{d}\tau}{\int_0^t \rho(s(\tau),\tau)\, \mathrm{d}\tau} \tag{2}$$

evaluated along a trajectory generated with Hamiltonian $H'(\mathbf{r},t) = H(\mathbf{r}) + V(s(\mathbf{r}),t)$, converges in the long time limit to the unbiased probability density $\rho(s)$, when the potential $V(s,t)$ is defined in terms of $\rho(s,t)$ as

$$V(s,t) = k_B T \ln \rho(s,t). \tag{3}$$

This means that the external potential $V(s,t)$ converges to the free energy $A(s)$ inverted in sign. The resulting algorithm is summarized by the Eqs. 2 and 3. The former is a recursive relation that determines both the direction and the amplitude of the estimated probability density variation at time t in a history-dependent way, starting from any initial arbitrary $\rho(s,0)$ different from zero. The latter defines the external potential in terms of the actual $\rho(s,t)$. At variance with previous methods, this algorithm does not utilize predefined, constant-in-time corrections to the bias potential (Gaussian functions in metadynamics [5]) or to the density of states (modification factors in the Wang-Landau method [6]), but determines them in terms of the previous history of the system, and therefore, does not need to be adapted case by case to the system of interest. Moreover, it is founded on a single, non-equilibrium trajectory, reducing the computational burden of generating subsequent, quasi-equilibrium trajectories as prescribed by adaptive umbrella sampling methods [8,9].

As a first application of SHUS, the FES of the alanine dipeptide (see Fig. 1) in water solution as a function of the dihedral angles Φ and Ψ was studied [14]. A 10 ns simulation was performed in the constant volume constant temperature thermodynamic ensemble at room temperature with an explicit solvent model. The obtained FES, shown in Fig. 1, is concurring with

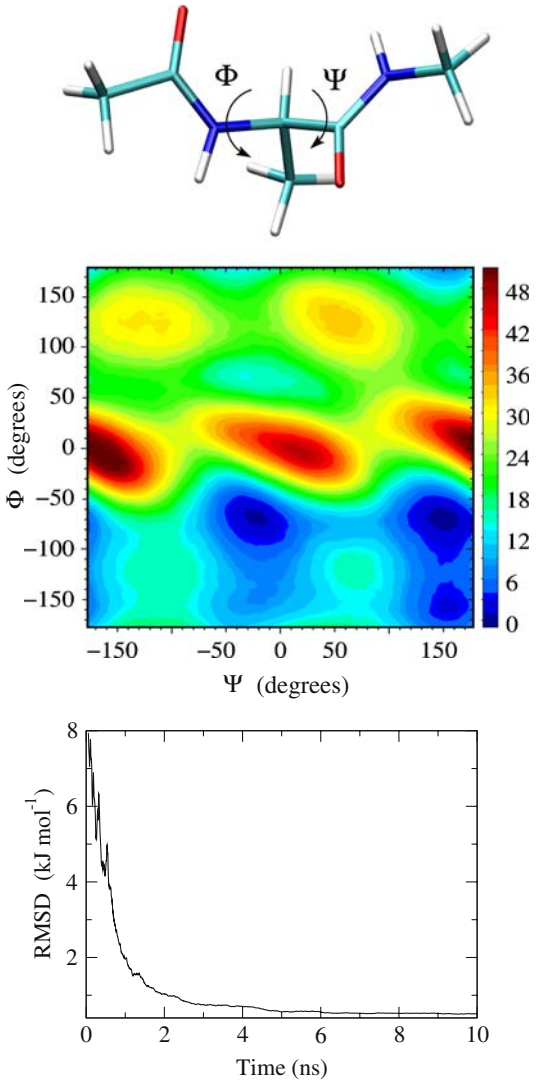

Fig. 1 *Upper*: schematic representation of the structure of the alanine dipeptide along with indication of the Ψ and Φ dihedral angles. *Middle*: FES of the alanine dipeptide as a function of Ψ and Φ calculated using SHUS [14]. *Lower*: Root mean square deviation of the SHUS-calculated FES from the reference FES (calculated using standard umbrella sampling technique) as a function of the sampling (simulation) time

previous theoretical works [5,15], showing the balance between the extended and the helical conformations of alanine dipeptide. The convergent nature of the bias potential $V(s,t)$ is depicted in the bottom of Fig. 1, where we report the root-mean-square deviation of the estimated FES from a reference one (obtained through standard umbrella sampling [16]) as a function of the sampling (simulation) time. The average error changes from 2 kJ mol^{-1} after 1 ns to 0.5 kJ mol^{-1} at the end of the simulation (we remark that convergence would seem to be reached even at half run time), showing both the qualitative and the quantitative predictive power of SHUS. The possibility of coupling this method with any of the pre-existing estimators of free energy differences, and its inherent parallelizability, give promising perspectives for its improvement.

2.2 Free energy from irreversible trajectories: studies on the Crooks relation

Among the methods devised for calculating FESs, the Jarzynski equality [17] and the correlated Crooks equation [18] (CE) are perhaps among the most intriguing because of their far reaching theoretical implications. In fact, they establish a strict correlation between two seemingly unrelated physical quantities, i.e., the work done on a system during irreversible transformations and the free energy difference between the final and the initial state of the transformations. Recently, a good deal of our efforts has been devoted to explore the potentialities of this type of approaches, with special attention to the CE (Eq. 10 of Ref. [18]). In fact, according to Ref. [18], Jarzynski equality can be derived from a more general relation (just the CE) occurring between the free energy difference of two states A and B (e.g., the states A and B could be characterized for having two different values of the distance between two given atoms) and the irreversible work done along an arbitrary trajectory for going from A to B. As proved in Ref. [19], the CE can be generalized in a more manageable form that allows to use it in practical experimental and computational cases [20,21]. Such form is the following:

$$P_{A\to B}(W) = P_{A\leftarrow B}(-W)\ \exp[\beta(W-\Delta F)], \tag{4}$$

where ΔF is the free energy difference between the thermodynamic states B and A, $P_{A\to B}(W)$ and $P_{A\leftarrow B}(-W)$ are the work distribution functions obtained from the forward and backward transformations, respectively, and W is the work done on the system in the forward transformation.

Our contribution [22] in the field has been to provide a theoretical demonstration of the CE in the context of constant volume, constant temperature steered MD simulations of systems thermostated by means of the Nosé–Hoover method [23] (and the so-called variant Nosé–Hoover chain [24]). In order to numerically verify the CE, tests on an isolated decaalanine peptide at finite temperature have been performed. In our tests, we have shown that the work distribution functions for the folding and α-helix unfolding of decaalanine do not necessarily have a Gaussian shape (signature of a Markovian process) as generally believed [21]. This is evident in Fig. 2, where we report the work distribution functions of both folding and unfolding transformations

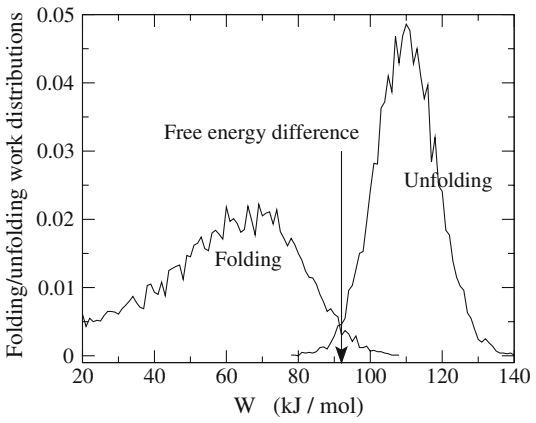

Fig. 2 Work distribution functions for folding and α-helix unfolding transformations of decaalanine [22]. The *arrow* indicates the free energy difference between the folded and unfolded states calculated by using thermodynamic integration

of decaalanine. Although the CE adapted to Gaussian work distributions [21] does not yield satisfactory results for the unfolding and (especially) folding of decaalanine, the use of the CE without any assumption on the shape of the work distributions (Eq. 4) allows to recover very precisely the exact folding/unfolding free energy difference. In fact, the CE predicts that the work distribution functions for the forward and backward transformations have an intersection at a work W equal to the free energy difference ΔF. This feature is clearly observable in Fig. 2. These results (1) show that the dynamics of decaalanine is far from being Markovian and (2) provide a convincing numerical test of the validity of the CE for non-Markovian systems. We have also shown that the left tail of the forward work distribution is a crucial feature. This is so since it is in the left tail that, according to the CE, the shape of the backward work distribution is carved. For the same reasons, particular importance is also to be ascribed to the right tail of the backward work distribution. In the behavior of the tails of the work distributions we find, not only a great deal of thermodynamic information, but also valuable clues about the dynamical regime at the equilibrium typical of the underlying reaction coordinate.

3 Molecular dynamics of biomolecules

The interest of our laboratory in computational studies targeted on biomolecules is a quite recent history. The first works specifically aimed at the modeling of systems of biochemical interest started to appear in the literature five years ago and are dealing with the analysis of pair interactions of aromatic amino acids in vacuum [25] and various solvents [3,4]. In the same project framework, we carried out a statistical study [26] on a large database of protein structures (taken from the Protein Data Bank) to develop a knowledge-based potential (or potential of mean force) not only for pair interactions among the amino acid residues, but also for the interaction between the amino acid residues and the solvent. With such an analysis, we were able to quantify the relative contribution of all possible residue–residue pairs to the stabilization of a protein structure. By performing threading experiments, we also showed the importance of the residue–solvent interactions in stabilizing the native fold of the proteins. These studies provide significant insights into the physics of important regulatory mechanisms occurring in biochemistry. In this section, we describe in deeper details, our more recent researches regarding prion proteins. This is indeed a hot issue of the scientific research in the last two decades because of its direct and quite immediate implications in medical science.

The cellular prion protein (PrP^C) is a GPI-anchored glycoprotein, whose structural conversion into a misfolded isoform (PrP^{Sc}) is considered the key event of a vast class of neuro-degenerative diseases. The structure of PrP^C has been resolved for several animal species and consists of a disordered N-terminal tail and a globular domain made up of three α-helices and a small antiparallel β-sheet. The insolubility of PrP^{Sc} has instead prevented the use of NMR or X-ray experiments to determine its structure. Even if some structural constraints for PrP^{Sc} structure are provided by spectroscopic [27], immunochemical and electron microscopy experiments [28,29], a high resolution structure of PrP^{Sc} is still unavailable and different models have been proposed [28–30]. The interconversion between the two prion isoforms is a complex process that takes place on time scales exceeding the predictive power of full-atom MD simulations. However, particular point mutations and/or physico-chemical conditions experimentally favor the pathogenic isoform and strongly accelerate misfolding [31,32]. It is therefore possible to gain insights in the first stages of the misfolding mechanism implementing these pathogenic perturbations in MD simulation and studying the minor unfolding events or local instabilities induced in PrP^C fold. Following this approach in the recent years many papers have been presented, focusing on the effect of various point mutations [33,34], high temperature [34,35], acidic pH [30,35–39] on PrP^C fold stability. Unfortunately, due to the size of the system and the complexity of the underlying FES, even studying the very early steps of prion protein misfolding by MD simulations is a challenging task and contradictory results have been published [30,36,37].

In our works [40,41] we used MD simulation techniques to study the effect of D178N point mutation on the stability of mouse PrP^C antiparallel β-sheet. In all simulations the prion proteins were modeled with AMBER-type potential models (Amber95 [42] in Ref. [40] and Amber03 [15] in Ref. [41]), while the TIP3P model [43] was used for water. The simulations were carried out in the isothermal-isobaric ensemble at room conditions using a cubic box with standard periodic boundary conditions. It is worth noting that periodic boundary condition methodologies, although widely used, can provide unphysical correlations due to the artificial periodicity of the system. These correlations are quite negligible when ordered solids or homogeneous fluids are considered, but are likely to become more relevant in the case of solute-solvent systems like ours, especially when a polar or charged solute is concerned. Such spurious effects could be removed using mean field approaches with spherical boundary conditions [44], which, on the other hand are always affected by explicit boundary effects due to the macroscopic character of the approximations used in the derivation of the mean field. However, such boundary effects can be limited either considering rigorous mean fields [45] or increasing the size of the box that confines the explicit molecules. Between these possible choices, we opted to use the periodic boundary based approach, eliminating the residue electric charge on the prion proteins by smearing the excess charge (inverted in sign) over all the atoms of the protein. An alternative way to get electroneutrality in the system would be that of adding an appropriate number of counterions arbitrarily distributed in the simulation sample. Although this last procedure is often used in standard simulations, we do believe that, perturbations of the solute due to the added counterions might yield uncontrolled structural changes. Consistently with the adopted boundary conditions, we treated the electrostatic interactions by the Ewald method with the smooth particle mesh algorithm [46].

The mutation D178N we have considered is associated to various inherited forms of transmissible spongiform encephalopathies, and it has been proved to lessen PrP^C folding free energy by urea-induced unfolding experiments [47]. In a first stage [40], we tried to determine the effect of this mutation on PrP^C fold through a comparative study of wild type PrP^C and its D178N mutant. Since PrP^{Sc} is known to be highly hydrophobic, we simulated the two systems both in water solution and in an extremely apolar environment (CCl_4 solution). In order to reduce sampling difficulties, multiple MD trajectories were generated for each system and non conventional thermalization schemes were adopted [40]. Even if in the nanosecond time scale only a very limited conformational flexibility was observed, we detected a significant weakening of PrP^C antiparallel β-sheet in the D178N mutant. This mutation-driven destabilization occasionally resulted in a complete break-up during some of the CCl_4 simulations, whereas in water solution the same feature was observed only to a minor extent. We concluded that, as this structural motif is destabilized in pathogenic conditions, it is likely to undergo disruption during the early stages of PrP^C misfolding. Our findings were at variance with conclusions presented in other MD simulation-based investigations [30,36], but in agreement with the parallel β-helix model proposed by Prusiner's group [28,29]. In a further study [41] (made in collaboration with the research group of Michele Parrinello of ETH Zurich, Switzerland), in order to definitively assess this problem and to quantify the effect of the D178N mutation in a more realistic environment, we decided to perform metadynamics MD simulations of wild type PrP^C and its mutant in water solution. Metadynamics method [5] is a powerful tool for exploring FESs along collective degrees of freedom. A characteristic feature of this method is the introduction of a history-dependent bias potential that greatly enhances the sampling along the chosen reaction coordinates. Furthermore, under the assumption that the other degrees of freedom are correctly sampled, it is also possible to reconstruct the underlying FES [5,48]. In our study, we developed a collective reaction coordinate based on backbone H-bonding geometry, to investigate the disruption/growth of PrP^C antiparallel β-sheet. We performed several metadynamics runs to evaluate the FES associated to this process, both for wild type PrP^C and its D178N mutant in water solution. The resulting profiles, shown in Fig. 3, confirmed our previous hypothesis indicating that antiparallel β-sheet is significantly weakened by the point mutation also in water solution. Moreover, the increased sampling guaranteed by the history-dependent potential allowed us to quantify the correlation between β-structure destabilization and the weakening of the H-bond network involving residues Arg164, Tyr128 and Asp/Asn178 caused by side chain replacement. This network indeed represents a sort of safety mechanism that contributes to one of the first free energy barriers in the $PrP^C \rightarrow PrP^{Sc}$ transition, i.e., the antiparallel β-sheet unzipping.

4 Molecular dynamics of neat liquids

The study of neat liquid phases and the characterization of the intermolecular interactions in terms of specific molecule–molecule structural arrangements and dynamical properties are topics treated in a number of recent

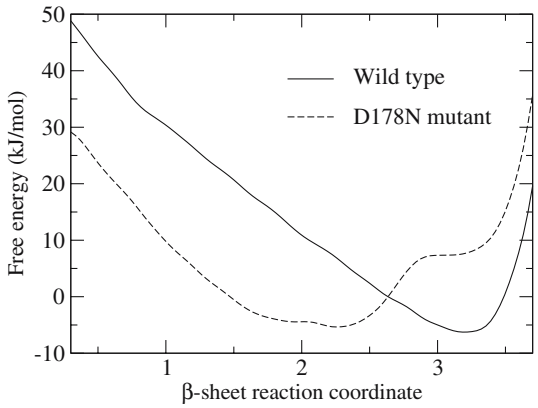

Fig. 3 Free energy as a function of the β-sheet reaction coordinate for the wild type PrP^C and its D178N mutant in water solution [41]. High values of the reaction coordinate indicate large β-sheet size and vice versa. The free energy curves are both arbitrarily set to zero for the reaction coordinate value of 2.63, which corresponds, on average, to a β-sheet formed by three residues

publications of our laboratory [49–60]. The use of simulation methods based on first principle MD [2] and/or on semi-empirical potentials [1] allowed us to gain either macroscopic information (e.g. optical properties) or microscopic/atomistic details (e.g. molecular linkage in H-bond networks of bulk phases) of the systems under study. Several types of molecular liquids have been investigated [53], but the most recent efforts have been devoted to systems able to form H-bonds [49–52,56–59]. In particular, molecular liquids that are representative members of a series of compounds or directly cover a special interest because of their own strategic role in chemistry or biochemistry have been considered. The studies on metatoluidine [56,57], formic acid [59], and pairs of aromatic molecules in various solvents [3,4] can be included in the former class of compounds, while in the latter class we may include methanol [51,61] and glycerol [49,50,52,58]. Other studies on this matter are currently in progress, including the MD simulation studies of liquid formamide and formic acid made in connection with the experiments carried by Roberto Righini (European Laboratory for Non-linear Spectroscopic, Firenze, Italy) and in collaboration with Shaul Mukamel (University of California, Irvine, USA). The research is specifically aimed at exploring the dynamical properties of these two liquids in terms of their non linear optical activity (two-dimensional infrared spectroscopy) from the perspective of the structural properties of the liquid phase.

4.1 H-bond networking: the case of glycerol

Since 1999, a good deal of work has been addressed to the study of glass-forming compounds that are peculiar systems, because, they give rise to a supercooled metastable liquid phase, where the dynamical behavior of the molecules becomes heterogeneous (i.e. the molecules form well-defined domains characterized by strongly different dynamics). This is the case of glycerol whose structural and dynamical properties have been analyzed by means of MD simulations in a wide range of temperatures, passing through the liquid-glass transition. After an exhaustive validation of the potential model [49], we have furnished a detailed description of the structure of the H-bond network of glycerol [50]. One of the main outcomes of the work has been the characterization of the H-bond network dynamics provided on the basis of an atomistic picture. We found, in particular, that the relaxation time of the H-bond network structure follows three regimes: a short ($\sim$1 ps), an intermediate ($\sim$10 ps) and a long time regime ($>$ 100 ps). These regimes have been correlated to well defined mechanisms that, in the order of increasing relaxation time, are: vibrational motion in the first neighbor's cage, structural reorganization of the cage, and molecular diffusion. Concerning the issue of the molecular structure in the bulk-phase, we also determined the concentration of the various conformers of glycerol. The results have been supported later on by further works made in our laboratory [52,62].

4.2 Liquid structure versus dynamical heterogeneity: the case of metatoluidine

The above studies [49,50] provided a quite complete scenario regarding the structure and the MD of glycerol, but did not give information about the occurrence of the dynamical heterogeneities typical of glass-forming liquids. This aspect is actually important, if one thinks that just the dynamical heterogeneity is believed to be the origin of the long time stretched exponential behavior of a number of dynamical properties in supercooled liquids. This issue has later been addressed in an investigation regarding metatoluidine [56,57]. More specifically, in Ref. [57], we reported results on the correlation between the structure of liquid metatoluidine and dynamical heterogeneity. The problem was approached observing that the pair molecular arrangement in supercooled metatoluidine (probed by the radial-angular pair distribution function, $g(R,\theta)$; see Fig. 4) shows maximum probability of pair arrangements, similar to those obtained from energy minimization of a single metatoluidine dimer (see circle in Fig. 4). We then divided the simulation sample into several arbitrary space domains and calculated, for each of them, the $g(R,\theta)$ function for H-bonded pairs and the time-dependent mean square displacement of the molecular centers of mass. Although each domain behaves very differently

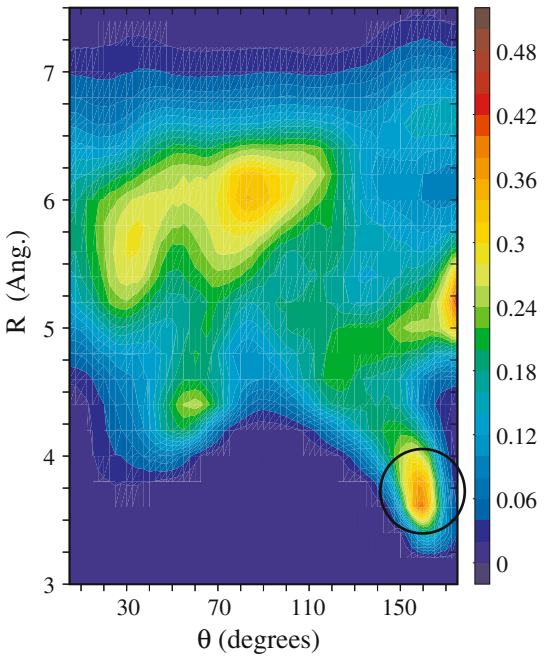

Fig. 4 Radial-angular pair distribution function [57] for H-bonded metatoluidine molecules calculated at 210 K. The radial part refers to the distance between the centers of mass, while the angular part refers to the angle between the normals to the aromatic rings. The *circle* marks the most probable pair configuration. The reference values for the chromatic scale are reported on the *right side* of the picture

with respect to the whole sample from both the structural and dynamical point of view, a clear correlation between the two quantities was observed. We found indeed that broad $g(R,\theta)$ functions are associated to large mean square displacements, while peaked $g(R,\theta)$ functions are typical of slow motion domains. Representative situations of two arbitrary domains are shown in Fig. 5. This suggests that dynamical heterogeneity in metatoluidine is correlated to the formation of energetically stable (H-bonded) molecular pairs, whose motion is slowed down by hindering effects acting on the pairs. Whenever the molecules do not experience strong pairing, the average molecular motion is faster.

4.3 What computer simulations can say on positron annihilation lifetime spectroscopy?

Further computational studies [58] on liquid glycerol have been carried out in collaboration with the research group of Josef Bartoš (Polymer Institute of Slovak Academy of Sciences, Bratislava, Slovakia). The research project has been basically addressed to provide a theoretical explanation for measurements of positron annihilation lifetime spectroscopy (PALS) [63]. The outcomes we gained hold for a generic molecular liquid, as further computational studies on propylene glycol have demonstrated (data to be published). In particular configurational snapshots of glycerol, taken from MD simulations of the liquid and glassy phases at various temperatures, have been explored by a virtual probing procedure to recover the free-volume data obtained by PALS (mean cavity volume). We found that, for glycerol (but also for propylene glycol), the calculated mean cavity volumes are much lower (about ten times) than those obtained from PALS (see Fig. 6). A deeper analysis of the MD trajectories demonstrated that reasonable agreement between experimental and calculated data can be achieved only assuming the existence of a lower limit for the volume of the cavities detectable by PALS measurements. For both glycerol and propylene glycol, this limiting volume is 25–30 $Å^3$ in the temperature range 250–275 K. We also found that the limiting volume for detectable cavities increases with increasing temperature. The comparison between experimental and calculated mean cavity volume is not feasible above 280 K. At this temperature, a significant bend of the mean cavity volume versus temperature curves has been observed experimentally that is absent in the calculated curve (see Fig. 6). Such a behavior has been interpreted [64] in the context of the α-relaxation mechanism described by the mode coupling theory [65]. In particular, Bartoš and coworkers have found that, at high temperature, the α-relaxation time of glycerol is lower than the ortho-positronium (positron + electron) lifetime, and therefore, a dynamic mechanism starts to become concurrent with the structural one. We so provided additional support to this empirical finding, showing the possible formation of very large free-volume cavities (cavity percolation through the simulation box), whose lifetime is too short to allow detection by PALS.

4.4 H-bonding in formic acid and methanol

In the framework of a research project on the structural and dynamical characterization of H-bond forming liquids, the recent MD simulation studies on the liquid phase of formic acid [59] and methanol [66] are worthy of mention. Regarding the former, ab initio and classical MD simulations have been performed to highlight the role of H-bonding, both on the global network structure of the liquid and on the local structure described in terms of molecular pairs arrangement. Formic acid is a formidable molecule because, despite its simplicity, it can give rise to a number of different H-bonds, i.e. C=O···H–O, H–O···H–O, C=O···H–C and H–O···H–C. In particular, liquid formic acid is one of the most representative systems where C–H···O bonds play a key role in the liquid structure. In fact we observed two

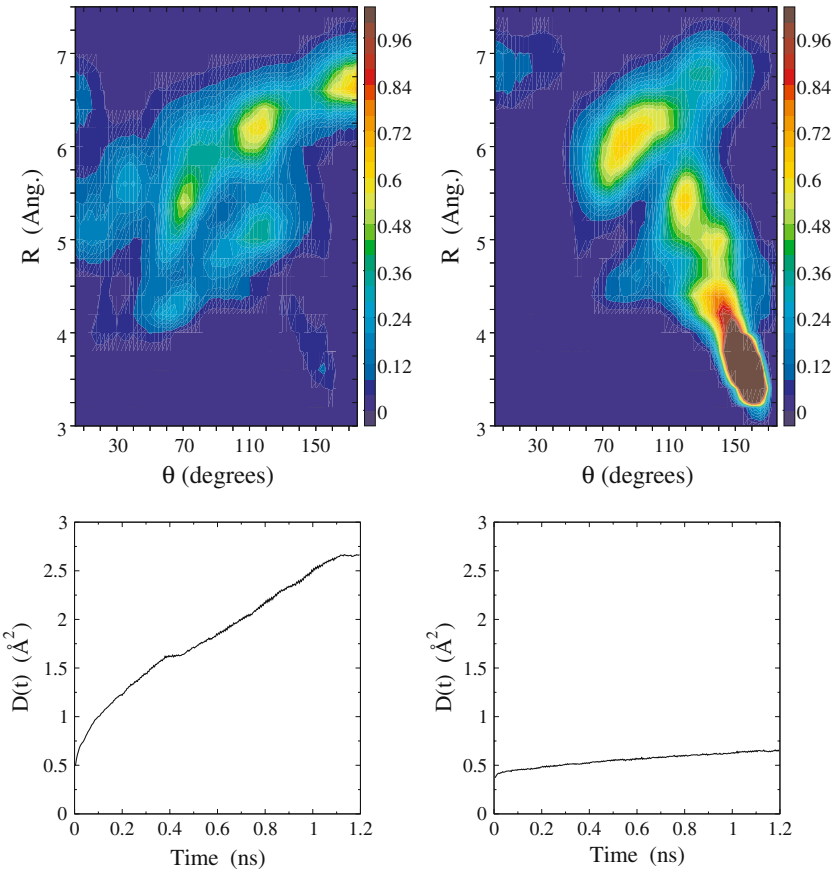

Fig. 5 *Upper*: radial-angular pair distribution functions of H-bonded metatoluidine molecules for two arbitrary space domains of the simulation sample [57]. *Lower*: time-dependent mean square displacement of the moleculear centers of mass belonging to the two domains

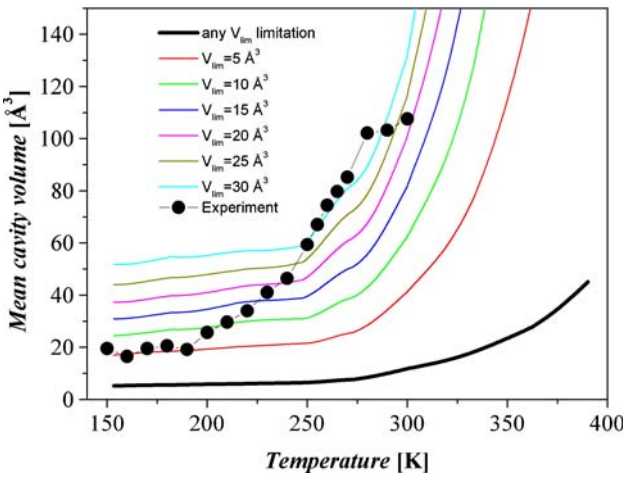

Fig. 6 Mean hole volumes from PALS measurements [64] and mean cavity volumes from MD simulations [58] (*bold line*) as a function of temperature. *Thin lines* refer to mean cavity volumes calculated [58] excluding cavities with a volume smaller than a given threshold V_{lim}

basic hierarchic structures in the liquid. The lower level structure is characterized by small O–H···O bonded clusters, whose size does not exceed 20–30 molecules. At the second level, the clusters are held together by weak C–H···O bonds forming an extended network. Furthermore, small H-bonded domains, in which about 20% of the molecules participate, are embedded in the network without forming C–H···O bonds. Moreover, an analysis focused on the determination of cyclic H-bonded dimers (typical pairing in gas phase [67]) has revealed that a significant concentration of such dimers (23% of molecules) occurs in the liquid. However, only a small number of molecules (about 3%) forms completely isolated dimers (i.e. non H-bonded with any other molecule in the sample). The resulting picture is that of a H-bond network of size comparable or even larger than that of the simulation box (500 molecules in the classical MD simulation). In contrast with other theoretical works [68], the parallel pair molecular arrangement has been found to be relevant. This preferential orientation is basically due to the O–H···O bonds and specifically to cyclic H-bond dimers. On the contrary, the C–H···O bonding is not found to favor any specific pair arrangement.

The MD simulation study of liquid methanol [66], together with the already discussed simulations on formic acid, gives a quite exhaustive view of a strongly

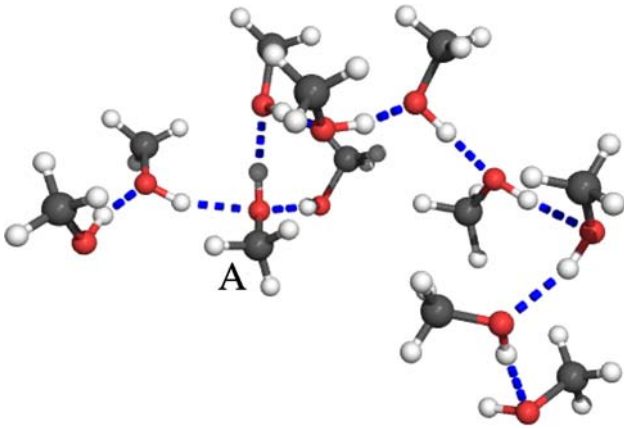

Fig. 7 Snapshot of a H-bond chain in liquid methanol taken from a MD trajectory [66]. The marked molecule forms a H-bond bifurcation

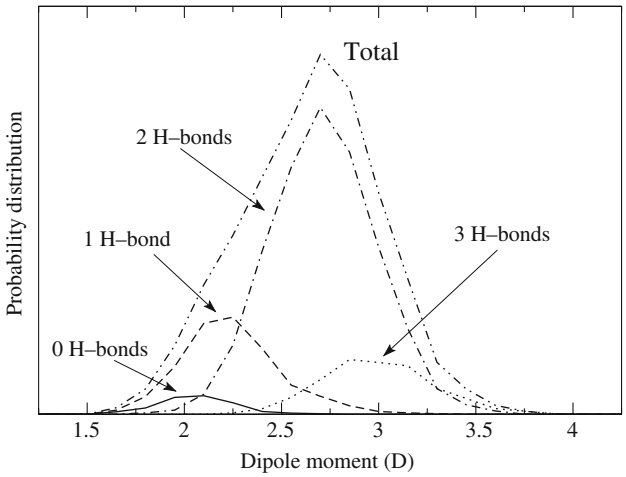

Fig. 8 Distribution functions of the molecular dipole moment in liquid methanol [66]. The various curves are calculated considering molecules forming a given number of H-bonds (reported on the *graph*)

self-associating liquid. Methanol has a wide biochemical interest (it is also a representative member of the alcohol series) and for this reason has attracted a great attention from both the experimental and the theoretical standpoint. This liquid, like formic acid, gives rise to an extended H-bond network with a significant presence of bifurcations (see Fig. 7). In fact, the number of methanol molecules involved in three H-bonds was found to be comparable to the number of molecules that form only one H-bond. However, the bulk structure of methanol, because of its lower capability to form multiple H-bonds with respect to formic acid, is made of H-bonded chains with smaller length (∼10 molecules). As observed for liquid formic acid, the complexity of aggregation of liquid methanol is further enhanced by the presence of a weaker directional H-bond interaction of the C–H$\cdots$O type. The dynamics of the H-bond has been characterized through the evaluation of its lifetime that is estimated to be about 1.9 ps in good agreement with experiments [69]. Moreover, the H-bonding dynamics includes also a shorter time regime (∼0.5 ps) that should be associated with a modulation due to librations of the molecular pairs.

A noteworthy finding in this system is the correlation between H-bonding and molecular polarization effects that have been investigated by the evaluation of the changes of the molecular dipole moment with the H-bond connectivity. Interestingly, it has been observed that the average dipole moment of a methanol molecule involved in only one H-bond does not change much, compared to a non H-bonded molecule. The dipole moment increases in fact by only 0.18 D. A relevant increase of the dipole moment (0.47 D in average) is instead found when a second H-bond is established. The formation of a third H-bond brings to a further average increase in the dipole moment by 0.28 D. The effect of the H-bond connectivity on the dipole moment is elucidated in Fig. 8.

4.5 Intermolecular charge transfer in H-bond forming systems

The non linear cooperative effect on the molecular polarizability observed in liquid methanol (see discussion in Sect. 4.4) has been also the object of a recent article [70] regarding two homologous series of water chains. By means of ab initio methods and a polarizable force field approach [71], we observed a significant increase in molecular polarization due to cooperative induction effects. We suggested that in the case of water chain configurations with favorable H-bond geometries, a significant contribution to electrical induction may arise from intermolecular charge transfer. A similar investigation, based on the SIBFA polarizable model [72], is currently in progress in collaboration with the research group of Nohad Gresh (Laboratoire de Pharmacochimie Moléculaire et Cellulaire, Paris, France). Following the same guideline, an investigation has been performed on various clusters (from dimers to pentamers) and on few liquid phase configurations of methanol and water [73]. Using ab initio calculations and a polarizable model based on the chemical potential equalization principle [74], we have highlighted the importance of intermolecular charge transfer in such systems. The charge transfer revealed through dipole moment calculations appears more relevant in small clusters than in the bulk phase. This is ascribed to the fact that bulk-phase disorder in water and methanol reduces intermolecular

charge transfer because of a sort of equilibrium between ingoing and outgoing flux of charge to and from a molecule.

5 Ions in methanol

The interactions of ions with solvent molecules strongly influence colligative properties of solutions, chemical reactivity and many phenomena of technological and biochemical interest as well. For this reason, a growing interest has been devoted to the study of the structural and dynamical properties of ions in polar solvents. A large part of the studies has been devoted to analyze water as solvent with a minor attention to other solvents. In our group we have started a systematic series of studies of the properties of simple ions in another important solvent like methanol, with interest in two anions [75,76] (Cl^- and Br^-), three alkaline cations [75,77] (Li^+, Na^+ and K^+) and two alkaline-earth cations [78] (Mg^{2+} and Ca^{2+}).

The interactions of ions with polar solvents are not simple to be modeled using semiempirical potentials due to the strong polarization of the first solvation shell and to the charge transfer. These systems have been approached successfully using ab initio MD employing density functional theory (DFT) with generalized gradient approximation (GGA) functionals. The method requires considerable computational resources that limit the possible system size and the length of the phase space exploration. The main results obtained in these studies concern the structure of the solvent in the first solvation shell and its stability, the charge transfer and the H-bond formation between anions and solvent molecules.

All the calculations have been performed with the CPMD code [79] in a cubic cell (12.05 Å side with 25 methanol molecules and one ion) with periodic boundary conditions using the BLYP functional [80,81] along with a plane wave expansion limited to 70 Ry. The integration time adopted has been 5 au (~0.12 fs) and the fictitious electronic mass was set to 800 au since deuterium isotope has been used. The pseudopotential is of the Martins–Troullier [82] type for C and O, while for the deuterium a Car-von Barth pseudopotential [83] was chosen. Using these conditions the structural and dynamical properties of liquid methanol are reproduced with a high degree of accuracy [66]. Both the Cl^- and Br^- anions have been described by Martins–Troullier [82] pseudo potentials. The pseudo potentials for alkaline ions (Li^+, Na^+ and K^+) have been chosen of the Goedecker type [84–86]. For both Mg^{2+} and Ca^{2+} cations, semi-core pseudopotentials of the Goedecker type [84–86] have given the best results.

The structure of the solutions has been analyzed mainly on the basis of pair distribution functions, the electronic properties have been obtained on the basis of the maximally localized Wannier functions (MLWF) [87–89] and the charge transfer analyzed on the basis of the atom in molecules (AIM) formalism [90].

One of the problems in Car Parrinello MD simulations [2] is represented by the transferability of the pseudopotentials. To validate the choice of the pseudopotentials for the ions and the plane wave cutoff, a series of cluster calculations (ion+methanol) have been performed using different pseudo potentials and compared with all electron calculations with the same functional along with an extended localized Gaussian basis set, 6-311++G(3df,3dp), and at the MP2 level. All electron calculations were performed using the Gaussian 98 suite of programs [91].

The chloride and bromide anions have been found to differ substantially as to the stability of the the first solvation shell, with a coordination number of 3.56 and 4.01, respectively. These values are in good agreement with the experimental results of 3±1 [92] and 3.7 [93,94]. The dynamical behavior of the first solvation shell is quite different in the two cases. While for the bromide the same 4 molecules are H-bonded to the anion, all along the simulation run of 9 ps, the chloride solution shows a variety of structures ranging from one to five molecules H-bonded to the anion with four being the most probable coordination number. This has been attributed to the higher radius of the bromide ion that allows more methanol molecules to form H-bonds without reciprocal repulsion. It can be remarked that previous classical simulations strongly overestimated the coordination numbers [92,95]. This large discrepancy has been attributed [92] to the lack of polarization effects in semiempirical potentials. Our work has shown that the methanol molecules are H-bonded to the anions and a charge transfer is present. The charge is essentially transferred to the methanol molecules of the first solvation shell and the amount is almost equal in the two cases ($\Delta q(e^-)$=0.24 for Cl^- and 0.28 for Br^-).

For the alkaline ions the coordination number obtained increases with the atomic number being 4.0, 5.0 and 5.4 for the lithium [75], sodium and potassium ions [77], respectively. It is interesting to note that for the lithium ion, that is the less polarizable, the same value has been obtained as from semiempirical calculations [95]. The value of 4 is in perfect agreement with recent Electron Spray measurements followed by infrared measurements [96]. From X-rays scattering measurements [97] a value of 6 was proposed; this higher value can be explained by the low elastic scattering coefficient of the lithium ion that does not allow for

a good localization of this species. It is interesting to note that for both Li^+ and Na^+, the same solvent molecules (4 and 5, respectively) stay in the first solvation shell all along the simulation runs (about 8 ps) while in the case of K^+ only 3 molecules are always in the first shell, 2 are exchanged only for a short time (<0.2 ps) and 4 have a very short residence time. This can be related to the larger radius of K^+ that allows for a greater number of molecules to approach to the ion at the same time but the overcrowding is such that they cannot be stably bonded in the first solvation shell. The amount of charge formally transferred from the solvent to the ions has been calculated and the resulting effective charge on the ions is ∼0.8 e^- on Li^+ and ∼0.9 e^- on Na^+ and K^+. The average charge on the methanol molecules as a function of the distance from the ion has also been calculated and it has been found that the first solvation shell is made up of negatively charged molecules while the second shell is positively charged. This is due to the combined charge transfer from the first shell to the ion and from the second to the first shell through the H-bond network.

A similar behavior has been found in alkali-heart ions [78] (Mg^{2+} and Ca^{2+}). In both cases, the coordination number is 6 and once the most stable structure is obtained, this is kept for more than 8 ps. For these two cations, simulations with 40 methanol molecules have also been performed and it has been found that size effects do not affect the first solvation shell structure in an appreciable way.

6 Chemical reactions and the blue moon ensemble

Chemical reactions are often rare events with reference to the feasible simulation times; therefore, an accelerating technique is necessary to explore the phase space in a reasonable simulation time. The blue moon ensemble [98,99] is one of the most successful techniques to study a chemical reaction when the reaction path can be described by a simple generalized coordinate. This method has been applied in combination with ab initio MD [2] to study chemical reactions in gas phase and subsequently in solution. The advantage of this approach is to study the reactions in the same thermodynamic conditions of the experiments and to have a direct evaluation of the thermal effects. Generally, the use of GGA functionals allows to reach a good accuracy in large part of the phase space. The only exceptions are represented by the strong underestimation of the dispersive forces [100] and to the excessive stabilization of the transition state in S_N2 reactions [101].

To evaluate the accuracy of the method, we started with simple reactions in the gas phase, where comparison with calculations at higher level of theory is possible. The first work of this kind was the study [102] of the bimolecular nucleophilic substitution (S_N2) $Cl^- + CH_3Br \longrightarrow CH_3Cl + Br^-$. In this work the variation of the molecular dipole moment along the reaction path was monitored showing a variation by a factor larger than 2.

This type of calculations has been extended to other S_N2 reactions in gas phase [103–110] including the effect of micro-solvation with water molecules, the effect of the α-substituent, the internal micro solvation and the competition between substitution and elimination. To increase the accuracy, the standard functional adopted in ab initio MD, i.e. BLYP, was substituted by other functionals and in particularly in the HCTH functional [111]. The failure of the BLYP was particularly evident in the S_N2 reaction $F^- + CH_3Cl \longrightarrow CH_3F + Cl^-$ that is almost barrierless with this functional while, albeit the barrier is still underestimated, the reaction path is correctly described using the HCTH functional [107].

The first reaction studied in water in our group was the S_N2 reaction [112] $Cl^- + CH_3Br \longrightarrow CH_3Cl + Br^-$. In this work, the attention was focused on the transition state and in particular on the H-bonds with water. The use of a more efficient function to analyze the lifetime of a H-bond was introduced.

Recently, our attention has been devoted to more complex reactions in solution. The free energy profile of methylene glycol dissociation to give formaldehyde in water was studied and it was shown that the whole hydration shell is involved cooperatively in the reaction. A particular attention was devoted also in this case to the characterization of the H-bond with formaldehyde [113]. In Fig. 9, a snapshot of the simulation is reported showing the MLWF [87–89] centers. It has been found that the H-bonds with the water molecules increase the dipole moment of formaldehyde that can be greater than 4 D (at the same level of theory the isolated molecule has a dipole moment of 2.64 D).

Among the chemical reactions presently under investigations we may mention a study of the pK_a of oxazole in water, with a simulated system consisting initially of a hydrogenate oxazole in a cubic cell with 36 water molecules. The nitrogen–hydrogen distance has been chosen as reaction coordinate and it has been increased in each simulation in the NVT ensemble by 0.1 Å till full dissociation. Integrating the mean constraint forces the free energy change has been computed obtaining a value of the pK_a in good agreement with experiments [114]. Another project that is being developed concerns the hydrolysis reaction of di-borane in water. The sample is made up of a di-borane molecule and 64 water molecules in a cubic box with periodic boundary conditions. The Perdew–Burke–Ernzerhof (PBE) functional

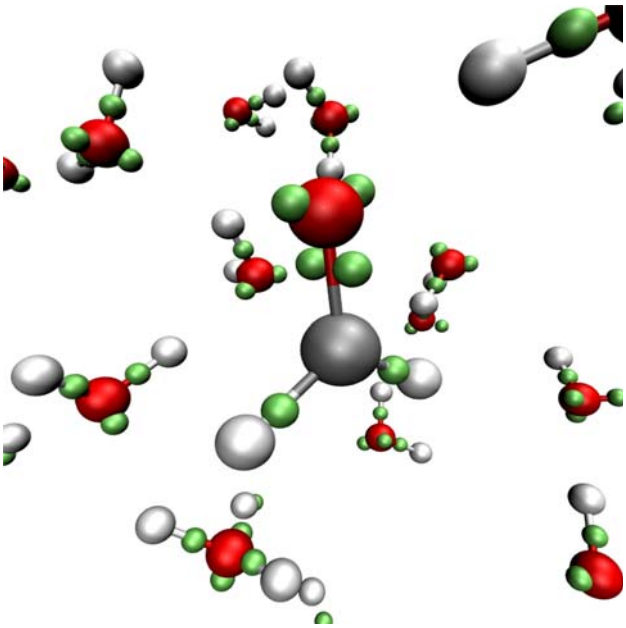

Fig. 9 Snapshot taken from the simulation of the formaldehyde in water. The Wannier center positions are reported in *green*

[115,116] along with Vanderbilt ultra soft pseudo-potentials [117–119] have been adopted. The boron–boron distance (B–B) has been constrained at increasing values, from 1.7 to 3.3 Å, performing 17 simulations to obtain the free energy profile. When the B–B distance reaches 2.6 Å, a water molecule starts to form a B–O bond and a BH_4^- species is formed [120]. The calculated free energy compares reasonably with experiments.

7 Metadynamics and solid state phase transitions

Solid state phase transitions under high pressure are of considerable interest to understand the behavior of matter under extreme conditions. High progress in this field has been obtained experimentally by the advent of the diamond anvil cell [121]. Nevertheless, experimentally it is not easy to obtain information on the modifications of the interatomic interactions and of the electronic distribution that occurs at high pressure, and a computational approach based on ab initio MD can be very useful in this respect. However, processes like solid state phase transitions at high pressure are to be considered rare events [122] characterized by high activation barriers or entropic bottlenecks and this will imply an unfeasible amount of simulation time to generate trajectories of this kind [1].

Many different techniques have been proposed to obtain a more efficient exploration of the FES. We have chosen to adopt the metadynamics [5,123] approach (MTD) introducing a new version of the method where the Parrinello–Rahman [124] and the MTD extended Lagrangian [123] are used together to follow solid state transitions. This new approach has been initially applied to study the high pressure transformation of lithium hydroxide [125]. The simulation was started from the ambient crystal structure, phase II (tetragonal, space group P4/nmm), with two asymmetric units in the primitive cell [126,127], using as collective variables the six cell parameter. After 15 ps simulation run, the system starts to explore a new phase. This new phase was characterized and its spectroscopic properties were found to be very similar to those of experimental phase III. The new phase is metastable at ambient conditions and we called it phase III′. Increasing the pressure of 100 kbar and performing a second MTD simulation after a few ps, the stable phase III was obtained. The transformation from phase II to phase III was essentially due to a compression along the c axis, that is perpendicular to the atomic layers in phase II. This new phase is characterized by the presence of H-bonds, absent in phase II, that are the source of the red shift and of the characteristic features observed in the OD stretching region both in the IR and Raman spectra.

Using a similar approach, it was possible to determine the crystalline structure of the high pressure phase of $LiOH{\cdot}H_2O$ starting from the known ambient conditions structure and to discuss the assignment of the external modes in both phases, [128]. The change in the molecular dipole of water with the phase transition was characterized by the MLWF [87–89] and in both phases, an average value of 3.6 D was found, considerably larger than the value obtained using the same approach for liquid water [129,130] (2.95 D).

Calculations on the high pressure phase diagram of nitrogen are now in progress. Our calculations were initially started from the recently proposed ζ phase structure [131], but we found it was unstable in the NVT ensemble independently of the functional adopted [132]. The calculations have been therefore started again using the lower pressure phase ϵ that was instead found stable. Since dispersive interactions, that are strongly underestimated by GGA functionals, are more important at lower pressure, we concluded that there are some problems with the proposed [131] structure for the ζ phase. Recently this was confirmed by a further analysis of the experimental data [133].

8 Reactions under high pressure

In recent years, a research project has been developed in our laboratory on chemical reactions at very high pressure (above 1 GPa) of simple unsaturated hydrocarbons and aromatics using an equipment based on

the diamond anvil cell [121,134]. In these conditions condensation and polymerization reactions occurs spontaneously. It has been found that high pressure reactions can lead to high quality polymers as far as the conformation and crystallinity of the products are concerned. The selectivity of the high pressure reactions pathway can be significantly enhanced when the pressurization is accompanied by additional activation methods and in particular, by laser excitation at appropriate wavelenghts, implying that the reactions occur with participation of excited electronic states. The mechanisms of the reactions and the microscopic interpretation of the high pressure thresholds remain open questions. To answer these problems a series of computational studies have been carried out by ab initio MD with the Car Parrinello method [2] as implemented in the CPMD code [79]. This approach has been proved to be effective for high pressure reactions in the seminal papers by Bernasconi et al. [135,136] on acetylene polymerization.

Calculations have been carried out in disordered condensed phases (propene [137], butadiene [138] and ethylene [139]) and in the crystalline state (ethylene [139], acetylene [140] and benzene [141]). The adopted level of theory is DFT in the GGA approximation that gives for the ground electronic state results comparable in accuracy with MP2 methods using large Gaussian basis sets. The natural choice for ab initio calculations in condensed phases is the expansion of the wavefunction at the Γ point of the Brillouin zone in plane waves making the expansion manageable by adopting pseudopotentials. The cutoff of the plane wave expansion has been set to guarantee at least 5% accuracy on the structure of the isolated molecules in the same conditions.

With the only exception of benzene [141], all the reactions have been studied in the NVT ensemble performing a series of simulations at increasing density. This approach shows the drawback that after the reaction is started, the pressure decreases and eventually, the polymerization is terminated before a quantitative transformation of the sample. The small size of the simulated samples can influence the length of the polymer. An additional technical problem lies in the high uncertainty in the value of the pressure due to the finite expansion of the plane wave basis set that gives rise to the Pulay stress. For this reason, we have generally preferred to discuss the results as a function of the simulation box volume or the sample density instead of the pressure. To overcome the high reaction barriers in a feasible simulation time, the standard approach is to over pressurize the system. Calculations have been carried using both the spin-restricted and spin-unrestricted formalism in order to be certain that the resulting reaction mechanism (ionic or radicalic) is unbiased by the computational approach.

In agreement with expectations, the electronic structure of the molecules is strongly perturbed at high pressure. The narrow distribution of the electronic density of states, characteristic of the isolated molecules, broadens considerably with increasing density and the HOMO-LUMO gap reduces. Therefore, mixing of the ground and excited states can be induced at higher pressures by thermal fluctuactions. The electronic rearrangement in the sample before the onset of the reaction and during the reaction has been followed through the MLWF [87–89] that allow to monitor the migration of the electron doublet, or of single electrons in the spin-polarized simulations.

With the exception of acetylene [140], the high pressure polymerizations have been found to occur by an ionic mechanism. Before the onset of the reaction, the perturbation of the electronic structure results in a charge separation and formation of zwitterionic species. This ensures a head to tail condensation and subsequent propagation of the reaction in a large part of the system. Ionization or formation of polar species is known as a typical response of a system to high pressure since it ensures a tighter packing of the molecules. The sample polarization has been monitored by the dipole moment of the monomers before the onset of the reaction. For instance, in the case of butadiene [138] an average dipole moment of 0.7 D has been obtained with a distribution extending up to 3 D. It has been found that the system size does not affect the reaction mechanism but only the lenght of the polymeric chain which, as already observed above, is also determined by the reduction of the sample pressure as the reaction proceeds. It is rewarding to note that the simulation of disordered samples of ethylene [139] produces only linear chains of oligomers, whitout branching, in good agreement with experimental findings [142]. Also in the case of butadiene the reaction products of the simulation [138] are in agreement with experiments [143].

In the simulations carried so far, the high pressure reactions exhibit a collective character. The changes in the electronic structure, that are the leading prerequisite for the reactivity, arise from the overall intermolecular interactions in the system and the single reactive events involve in general more than two molecules. An evidence of the collective character of the reaction is also obtained from the mutual orientation of the dipole moments induced in the molecules. It is also of interest that the spread of the MLWF substantially increases in the involved electrons during the reaction. For instance, in the case of propene, values higher than 4 au have been obtained (see Fig. 10). This is an evidence of a strong electron delocalization during the reaction.

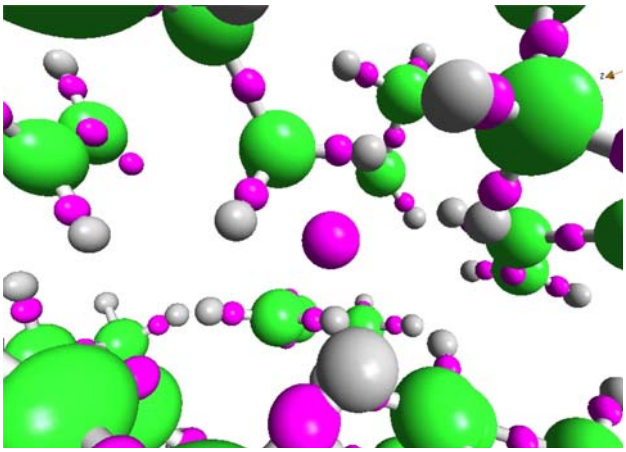

Fig. 10 Snapshot of a propene reaction simulation. In *purple* the Wannier center positions are reported. A Wannier center characterized by a large spread and not localized on a molecule is shown in the middle of the figure

In all the simulations, it has been found that the reaction occurs when the C-C intermolecular separation reduces below a certain threshold, as a concurring effect of the decrease of the equilibrium intermolecular distance and of the mean square vibrational displacement. This point has been investigated with particular attention for the benzene amorphization [141] where the reaction has been studied at various P-T conditions and the equation of state is known. Both experiments and simulations indicate that the reaction occurs when the intermolecular distance decreases below 2.6 Å. This is the counterpart of the macroscopic pressure – temperature reaction threshold and could allow to foresee the conditions for the reaction when the equation of state is available.

In the crystalline state, the effect of geometrical constraints becomes very important. For the ethylene polymerization [139] at moderate pressure, the reaction propagates among molecules on equivalent sites in the crystal, giving rise to a linear polymer with no branching. This is a manifestation of the topochemical principle of solid state reactions [144] since the intermolecular distance and mutual orientation are the most favourable along one of the crystallographic axes. At higher pressure, because of the anisotropic compressibility, the intermolecular distances between equivalent and non equivalent molecules become comparable and the reaction propagates along two directions, giving a branched polymer. This computational result is in very good agreement with experiments [142,145].

Acknowledgements We are grateful to all co-authors for their fundamental contribution to the works published by our group and to the other coworkers who, with stimulating discussions and valuable suggestions, allowed us to improve the quality of our studies. This work was supported by the Ministero dell'Istruzione, dell'Università e della Ricerca (MIUR) and by the European Union (contract RII3-CT-2003-506350).

References

1. Frenkel D, Smit B (2002) Understanding molecular simulation. Academic, San Diego
2. Car R, Parrinello M (1985) Phys Rev Lett 55:2471
3. Gervasio FL, Chelli R Marchi M, Procacci P, Schettino V (2001) J Phys Chem B 105:7835
4. Chelli R, Gervasio FL, Procacci P, Schettino V (2002) J Am Chem Soc 124:6133
5. Laio A, Parrinello M (2002) Proc Natl Acad Sci USA 99:12562
6. Wang F, Landau DP (2001) Phys Rev Lett 86:2050
7. Darve E, Pohorille A (2001) J Chem Phys 115:9169
8. Hooft RWW, van Eijck BP, Kroon J (1992) J Chem Phys 97:6690
9. Mezei M (1987) J Comput Phys 68:237
10. Laio A, Rodriguez-Fortea A, Gervasio FL, Ceccarelli M, Parrinello M (2005) J Phys Chem B 109:6714
11. Wang F, Landau DP (2001) Phys Rev E 64:056101
12. Lee HK, Okabe Y, Landau DP (2006) Comp Phys Comm 175:36
13. Henin J, Chipot C (2004) J Chem Phys 121:2904
14. Marsili S, Barducci A, Chelli R, Procacci P, Schettino V (2006) J Phys Chem B 110:14011
15. Duan Y, Wu C, Chowdhury S, Lee MC, Xiong GM, Zhang W, Yang R, Cieplak P, Luo R, Lee T et al (2003) J Comput Chem 24:1999
16. Torrie GM, Valleau JP (1974) Chem Phys Lett 28:578
17. Jarzynski C (1997) Phys Rev Lett 78:2690
18. Crooks GE (1998) J Stat Phys 90:1481
19. Crooks GE (1999) Phys Rev E 60:2721
20. Collin D, Ritort F, Jarzynski C, Smith SB, Tinoco I, Bustamante C, (2005) Nature 437:231
21. Park S, Schulten K (2004) J Chem Phys 120:5946
22. Procacci P, Marsili S, Barducci A, Signorini GF, Chelli R (2006) J Chem Phys 125:164101
23. Hoover WG, (1985) Phys Rev A 31:1695
24. Tuckerman ME, Berne BJ, Martyna GJ, Klein ML (1993) J Chem Phys 99:2796
25. Gervasio FL, Chelli R, Procacci P, Schettino V (2002) PROTEINS 48:117
26. Chelli R, Gervasio FL, Procacci P, Schettino V (2004) PROTEINS 55:139
27. Pan K, Baldwin M, Nguyen J, Gasset M, Serban A, Groth D, Mehlhorn I, Huang Z, Fletterick RJ, Cohen FE et al (1993) Proc Natl Acad Sci USA 90:10962
28. Wille H, Michelitsch MD, Génebaut V, Supattapone S, Serban A, Cohen FE, Agard DA, Prusiner SB (2002) Proc Natl Acad Sci USA 99:3563
29. Govaerts C, Wille H, Prusiner SB, Cohen FE (2004) Proc Natl Acad Sci USA 101:8342
30. DeMarco ML, Daggett V (2004) Proc Natl Acad Sci USA 101:2293
31. Prusiner SB (1996) Trends BioChem Sci 21:482
32. Riesner D (2003) Br Med Bull 66:21
33. Gsponer J, Ferrara P, Caflisch A (2001) J Mol Graph Model 20:169
34. El Bastawissy E, Knaggs MH, Gilbert IH (2001) J Mol Graph Model 20:145

35. Gu W, Wang T, Zhu J, Shi Y, Liu H (2003) BioPhys Chem 104:79
36. Alonso DO, DeArmond SJ, Cohen FE, Daggett V (2001) Proc Natl Acad Sci USA 98:2985
37. Sekijima M, Motono C, Yamasaki S, Kaneko K, Akiyama Y (2003) BioPhys J 85:1176
38. Langella E, Improta R, Barone V (2004) BioPhys J 87:3623
39. Langella E, Improta R, Crescenzi O, Barone V (2006) PROTEINS 64:167
40. Barducci A, Chelli R, Procacci P, Schettino V (2005) BioPhys J 88:1334
41. Barducci A, Chelli R, Procacci P, Schettino V, Gervasio FL, Parrinello M (2006) J Am Chem Soc 128:2705
42. Cornell WD, Cieplak P, Bayly CI, Gould IR, Merz KM, Ferguson DM, Spellmeyer DC, Fox T, Caldwell JW, Kollman PA (1995) J Am Chem Soc 117:5179
43. Jorgensen WL, Chandrasekhar J, Madura JD, Impey RW, Klein ML (1983) J Chem Phys 79:926
44. Pavone M, Brancato G, Morelli G, Barone V (2006) Chem Phys Chem 7:148
45. Brancato G, Di Nola A, Barone V, Amadei A (2005) J Chem Phys 122:154109
46. Essmann U, Perera L, Berkowitz ML, Darden T, Lee H, Pedersen LG (1995) J Chem Phys 103:8577
47. Liemann S, Glockshuber R (1999) BioChemistry 38:3258
48. Bussi G, Laio A, Parrinello M (2006) Phys Rev Lett 96:090601
49. Chelli R, Procacci P, Cardini G, Della Valle RG, Califano S (1999) Phys Chem Chem Phys 1:871
50. Chelli R, Procacci P, Cardini G, Califano S (1999) Phys Chem Chem Phys 1:879
51. Chelli R, Ciabatti S, Cardini G, Righini R, Procacci P (1999) J Chem Phys 111:4218
52. Chelli R, Gervasio FL, Gellini C, Procacci P, Cardini G, Schettino V (2000) J Phys Chem A 104:5351
53. Chelli R, Cardini G, Procacci P, Righini R, Califano S, Albrecht A (2000) J Chem Phys 113:6851
54. Ricci M, Bartolini P, Chelli R, Cardini G, Califano S, Righini R (2001) Phys Chem Chem Phys 3:2795
55. Chelli R, Cardini G, Ricci M, Bartolini P, Righini R, Califano S (2001) Phys Chem Chem Phys 3:2803
56. Chelli R, Cardini G, Procacci P, Righini R, Califano S (2002) J Chem Phys 116:6205
57. Chelli R, Cardini G, Procacci P, Righini R, Califano S (2003) J Chem Phys 119:357
58. Račko D, Chelli R, Cardini G, Bartoš J, Califano S (2005) Eur Phys J D 32:289
59. Chelli R, Righini R, Califano S (2005) J Phys Chem B 109:17006
60. Magro A, Frezzato D, Polimeno A, Moro GJ, Chelli R, Righini R (2005) J Chem Phys 123:124511
61. Pagliai M, Cardini G, Righini R, Schettino V (2003) J Chem Phys 119:6655
62. Chelli R, Gervasio FL, Gellini C, Procacci P, Cardini G, Schettino V (2000) J Phys Chem A 104:11220
63. Brandt W, Dupasquier A (1983) Positron solid state physics (North-Holland, Amsterdam)
64. Bartos J, Sausa O, Bandzuch P, Zrubcova J, Kristiak J (2002) J Non-Cryst Solids 307:417
65. Götze W (1991) Liquids: freezing and glass transition (North-Holland, Amsterdam)
66. Pagliai M, Cardini G, Righini R, Schettino V (2003) J Chem Phys 119:6655
67. Almenningen A, Bastiansen O, Motzfeldt T (1969) Acta Chem Scand 23:2848
68. Jedlovszky P, Turi L (1997) J Phys Chem B 101:5429
69. Gaffney KJ, Davis PH, Piletic IR, Levinger NE, Fayer MD (2002) J Phys Chem A 106:12012
70. Chelli R, Schettino V, Procacci P (2005) J Chem Phys 122:234107
71. Chelli R, Procacci P (2002) J Chem Phys 117:9175
72. Gresh N (1997) J Phys Chem A 101:8680
73. Chelli R, Pagliai M, Procacci P, Cardini G, Schettino V (2005) J Chem Phys 122:074504
74. Mortier WJ, Ghosh SK, Shankar S (1986) J Am Chem Soc 108:4315
75. Pagliai M, Cardini G, Schettino V (2005) J Phys Chem B 109:7475
76. Faralli C, Pagliai M, Cardini G, Schettino V (2006) J Phys Chem B 110:14923
77. Faralli C, Pagliai M, Cardini G, Schettino V (2006) Phys Chem Chem Phys (submitted)
78. Faralli C, Pagliai M, Cardini G, Schettino V (2006) (in preparation)
79. Hutter J, Alavi A, Deutch T, Bernasconi M, Goedecker S, Marx D, Tuckerman M, Parrinello M, (1995–1999) CPMD. MPI für Festkörperforschung and IBM Zurich Research Laboratory, Stuttgart
80. Becke AD (1988) Phys Rev A 38:3098
81. Lee C, Yang W, Parr RG (1988) Phys Rev B 37:785
82. Troullier N, Martins JL (1991) Phys Rev B 43:1993
83. Vuilleumier R, Sprik M (2001) J Chem Phys 115(8):3454
84. Goedecker S, Teter M, Hutter J (1996) Phys Rev B 54:1703
85. Hartwigsen C, Goedecker S, Hutter (1998) J, Phys Rev B 58:3641
86. Krack M (2005) Theor Chem Acc 114:145
87. Marzari N, Vanderbilt D (1997) Phys Rev B 56:12848
88. Silvestrelli P, Marzari N, Vanderbilt D, Parrinello M (1998) Solid State Commun 107:7
89. Silvestrelli PL (1999) Phys Rev B 59:9703
90. Bader WRF (1991) Chem Rev 91:893
91. Frisch MJ, Trucks GW, Schlegel HB, Scuseria GE, Robb MA, Cheeseman JR, Zakrzewski VG, Montgomery JA, Jr, Stratmann RE et al (1998) Gaussian 98, Revision A.11. (Gaussian Inc., Pittsburg, PA)
92. Sesé G, Guàrdia E, Padró JA (1996) J Chem Phys 105: 8826
93. Tanida H, Sakane H, Watanabe I (1994) J Chem Soc Dalton Trans 2321–2326
94. Watanabe I (1995) J Mol Liq 65/66:245
95. Impey RW, Sprik M, Klein ML (1987) J Am Chem Soc 109:5900
96. Wu C-C, Wang Y-S, Chandhuri C, Jiang JC, Chang H-C (2004) Chem Phys Lett 388:457
97. Megyes T, Radnai T, Grósz T, Pálinkàs G (2002) J Mol Liq 101:3
98. Carter E, Ciccotti G, Hynes J, Kapral R (1989) Chem Phys Lett 98:472
99. Sprik M (1998) Faraday Discuss. 110:437
100. Raugei S, Cardini G, Schettino V (1998) Mol Phys 95:477
101. Deng L, Branchadell V, Ziegler T (1994) J Am Chem Soc 116:10645
102. Raugei S, Cardini G, Schettino V (1999) J Chem Phys 111:10887
103. Raugei S, Cardini G, Schettino V (2001) J Chem Phys 114:4089
104. Pagliai M, Raugei S, Cardini G, Schettino V (2001) Phys Chem Chem Phys 3:2559
105. Pagliai M, Raugei S, Cardini G, Schettino V (2001) Phys Chem Chem Phys 3:4870
106. Pagliai M, Raugei S, Cardini G, Schettino V (2002) J Chem Phys 117:2199

107. Mugnai M, Cardini G, Schettino V (2003) J Chem Phys 118:2767
108. Mugnai M, Cardini G, Schettino V (2003) J Phys Chem A 107:2540
109. Pagliai M, Raugei S, Cardini G, Schettino V (2003) J Chem Phys 119:9063
110. Mugnai M, Cardini G, Schettino V (2004) Rend Fis Acc Lincei s.9, 15:99
111. Boese AD, Doltsinis NL, Handy NC, Sprik M (2000) J Chem Phys 112:1670
112. Pagliai M, Raugei S, Cardini G, Schettino V (2003) J Mol Struct THEOCHEM 630:141
113. Mugnai M, Cardini G, Schettino V, Nielsen CJ (2006) Phys Chem Chem Phys (Submitted)
114. Pratesi S (2006) Master's Thesis, Università di Firenze (in preparazione)
115. Perdew JP, Wang Y (1992) Phys Rev B 45:13244
116. Perdew JP, Burke K, Ernzerhof M (1996) Phys Rev Lett 77:3865
117. Vanderbilt D (1990) Phys Rev B 41:7892
118. Laasonen K, Car R, Lee C, Vanderbilt D (1991) Phys Rev B 43:6796
119. Laasonen K, Pasquarello A, Lee C, Car R, Vanderbilt D (1993) Phys Rev. B 47:10142
120. di Pietro E, Cardini G, Schettino V (2006) (in preparation)
121. Schettino V, Bini R (2003) Phys Chem Chem Phys 5:1951
122. Parrinello M (2000) Comput Sci Eng 2:22
123. Iannuzzi M, Laio A, Parrinello M (2003) Phys Rev Lett 90:238302
124. Parrinello M, Rahman A (1980) Phys Rev Lett 45:1196
125. Pagliai M, Iannuzzi M, Cardini G, Parrinello M, Schettino V (2006) Chem Phys Chem 7:141
126. Von Göttlicher S, Kieselbach B (1976) Acta Cryst. A32:185
127. Mair SL (1978) Acta Cryst A34:542
128. di Pietro E, Pagliai M, Cardini G, Schettino V (2006) J Phys Chem B 110:13539
129. Silvestrelli PL, Parrinello M (1999) Phys Rev Lett 82:3308
130. Silvestrelli PL, Parrinello M (1999) J Chem Phys 111:3572
131. Eremets M, Gavriliuk G, Serebryanaya NR, Trojan IA, Dzivenko DA, Boehler R, Mao K, Hemley R (2004) J Chem Phys 121:11296
132. Muniz F (2006) Master's Thesis, Univeristà di Firenze (in preparazione)
133. Gregoryanz E, Sanloup C, Bini R, Kreutz J, Jodl H, Somayazulu M, Mao K, Hemley R (2006) J Chem Phys 124:16102
134. Schettino V, Bini R, Ceppatelli M, Ciabini L, Citroni M (2005) Adv Chem Phys 131:105
135. Bernasconi M, Chiarotti GL, Focher P, Parrinello M, Tosatti E (1996) Phys Rev Lett 76:2081
136. Bernasconi M, Chiarotti GL, Focher P, Parrinello M, Tosatti E (1997) Phys Rev Lett 78:2008
137. Mugnai M, Cardini G, Schettino V (2004) J Chem Phys 120:5327
138. Mugnai M, Cardini G, Schettino V (2004) Phys Rev B 70:020101(1)
139. Mugnai M, Pagliai M, Cardini G, Schettino V (2006) (in preparation)
140. Pignataro G (2005) Master's Thesis, Università di Firenze
141. Ciabini L, Gorelli FA, Santoro M, Bini R, Schettino V, Raugei S (2006) Nature Mater (in press)
142. Chelazzi D, Ceppatelli M, Santoro M, Bini R, Schettino V (2004) Nature Mater 3:470
143. Citroni M, Ceppatelli M, Bini R and Schettino V (2002) Science 295:2058
144. Cohen M (1975) Ang Chem Int Ed Engl 14:386
145. Chelazzi D, Ceppatelli M, Santoro M, Bini R, Schettino V (2004) J Phys Chem B 109:21658